PHYSICAL REVIEW D **71,** 075002 (2005)

Supersymmetric origin of matter

C. Balázs,[1] M. Carena,[2] A. Menon,[1,3] D. E. Morrissey,[1,3] and C. E. M. Wagner[1,3]
[1]*HEP Division, Argonne National Laboratory, 9700 Cass Avenue, Argonne, Illinois 60439, USA*
[2]*Fermi National Accelerator Laboratory, P.O. Box 500, Batavia, Illinois 60510, USA*
[3] *Enrico Fermi Institute, University of Chicago, 5640 S. Ellis Avenue, Chicago, Illinois 60637, USA*
(Received 6 January 2005; published 5 April 2005)

The minimal supersymmetric extension of the standard model (MSSM) can provide the correct neutralino relic abundance and baryon number asymmetry of the universe. Both may be efficiently generated in the presence of *CP* violating phases, light charginos and neutralinos, and a light top squark. Because of the coannihilation of the neutralino with the light stop, we find a large region of parameter space in which the neutralino relic density is consistent with WMAP and SDSS data. We perform a detailed study of the additional constraints induced when *CP* violating phases, consistent with the ones required for baryogenesis, are included. We explore the possible tests of this scenario from present and future electron electric dipole moment (EDM) measurements, direct neutralino detection experiments, collider searches and the $b \to s\gamma$ decay rate. We find that the EDM constraints are quite severe and that electron EDM experiments, together with stop searches at the Tevatron and Higgs searches at the LHC, will provide a definite test of our scenario of electroweak baryogenesis in the next few years.

DOI: 10.1103/PhysRevD.71.075002 PACS numbers: 12.60.Jv, 14.80.Ly, 95.35.+d

I. INTRODUCTION

The nature of the dark matter and the source of the baryon-antibaryon asymmetry are two of the most important questions at the interface of particle physics and cosmology. Recent improvements in the astrophysical and cosmological data, most notably due to the Wilkinson microwave anisotropy probe (WMAP) [1] and the Sloan digital sky survey (SDSS) [2], have determined the matter and baryon densities of the Universe to be $\Omega_M h^2 = 0.135^{+0.008}_{-0.009}$ and

$$\Omega_B h^2 = 0.0224 \pm 0.0009, \tag{1}$$

respectively, with $h = 0.71^{+0.04}_{-0.03}$. Together these imply a (dominantly) cold dark-matter density of

$$\Omega_{\rm CDM} h^2 = 0.1126^{+0.0161}_{-0.0181}, \tag{2}$$

at 95% CL. Such precise determinations of $\Omega_B h^2$ and $\Omega_{\rm CDM} h^2$ impose severe constraints on any particle physics model that tries to explain one or both of these values.

The standard model of particle physics (SM) has been tested extensively by collider experiments, and has so far withstood all of them. However, the SM performs considerably worse when it comes to cosmology, and can account for neither the baryon asymmetry, nor the dark matter. Furthermore, in the SM, the electroweak scale is unstable under quantum corrections suggesting that an extension of the SM description is required at energies near the TeV scale. A particularly attractive way to stabilize the weak scale is to introduce supersymmetry [3]. Remarkably, the minimal supersymmetric extension of the standard model, the MSSM, can also explain the baryon asymmetry, and contains an excellent dark-matter candidate in the lightest supersymmetric particle (LSP).

The LSP of the MSSM is stable if *R*-parity is imposed. If, in addition, the LSP is neutral under $\mathrm{SU}(3)_C \times \mathrm{U}(1)_{EM}$, it is a candidate for cold dark matter. One such particle is the lightest neutralino. This particle tends to have a mass of order of the weak scale and electroweak strength couplings, and therefore naturally gives rise to a dark-matter relic density close to the measured value. The fact that a stable particle with electroweak strength couplings and mass of order 1 TeV naturally generates a relic density near the required value can be taken as further motivation for new physics at the TeV scale.

In general, any mechanism for baryogenesis must fulfill the three Sakharov requirements [4]; namely, baryon number (B) violation, *CP* violation, and a departure from equilibrium (unless *CPT* is violated, see for instance [5]). All three requirements are satisfied in both the SM and the MSSM during the electroweak phase transition, and this is the basis for electroweak baryogenesis (EWBG) [6]. However, as we will discuss below, while electroweak baryogenesis may be realized in the MSSM, SM processes cannot generate a large enough baryon asymmetry during the electroweak phase transition.

Baryon number violation occurs in the SM and the MSSM due to anomalous sphaleron transitions that violate $(B + L)$ [7]. These transitions are exponentially suppressed at low temperatures in the electroweak broken phase [8], but become active at high temperatures when the electroweak symmetry is restored [9]. In the absence of other charge asymmetries, like $(B - L)$, they produce baryons and antibaryons such that the net baryon number relaxes to zero, and so do not by themselves generate a baryon asymmetry [6,10]

If the electroweak phase transition is first order, bubbles of broken phase nucleate within the symmetric phase as the Universe cools below the critical temperature. These pro-

vide the necessary departure from equilibrium. EWBG then proceeds as follows [11]. *CP* violating interactions in the bubble walls generate chiral charge asymmetries which diffuse into the symmetric phase in front of the walls. There, sphaleron transitions, which are active in the symmetric phase, convert these asymmetries into a net baryon number. This baryon number then diffuses into the bubbles where the electroweak symmetry is broken. Sphaleron transitions within the broken phase tend to destroy the baryon number generated outside the bubble. To avoid this, the sphaleron transitions within the broken phase must be strongly suppressed. This is the case provided the electroweak phase transition is *strongly* first order [12],

$$v(T_c)/T_c \gtrsim 1, \tag{3}$$

where $v(T_c)$ denotes the Higgs vacuum expectation value at the critical temperature T_c.

The strength of the electroweak phase transition may be determined by studying the finite temperature effective Higgs boson potential. The Higgs vacuum expectation value at the critical temperature is inversely proportional to the Higgs quartic coupling, related to the Higgs mass. For sufficiently light Higgs bosons, a first-order phase transition can be induced by the loop effects of light bosonic particles, with masses of order the weak scale and large couplings to the Higgs fields. The only such particles in the SM are the gauge bosons, and their couplings are not strong enough to induce a first-order phase transition for a Higgs mass above the LEP II bound [13].

Within the MSSM, there are additional bosonic degrees of freedom which can make the phase transition more strongly first order. The most important contribution comes from a light stop, which interacts with the Higgs field with a coupling equal to the top-quark Yukawa. In addition, a light stop has 6 degrees of freedom, three of color and two of charge, which further enhances the effect on the Higgs potential. Detailed calculations show that for the mechanism of electroweak baryogenesis to work, the lightest stop mass must be less than the top mass but greater than about 120 GeV to avoid color-breaking minima. Simultaneously, the Higgs boson involved in breaking the electroweak symmetry must be lighter than 120 GeV [14–21], only slightly above the present experimental bound [22],

$$m_h \gtrsim 114 \text{ GeV}, \tag{4}$$

which is valid for a Higgs boson with SM-like couplings to the gauge bosons.[1]

The combined requirements of a first-order electroweak phase transition, strong enough for EWBG, and a Higgs boson mass above the experimental limit severely restrict the allowed values of the stop parameters. To avoid generating too large a contribution to $\Delta\rho$, the light stop must be mostly right-handed. Since the stops generate the most important radiative contribution to the Higgs boson mass in the MSSM [31], the other stop must be considerably heavier in order to raise the Higgs mass above the experimental bound, Eq. (4). For the stop soft supersymmetry-breaking masses, this implies [18]

$$\begin{aligned} m^2_{U_3} &\lesssim 0, \\ m^2_{Q_3} &\gtrsim (1 \text{ TeV})^2. \end{aligned} \tag{5}$$

A similar tension exists for the combination of soft SUSY breaking parameters defining the stop mixing, $|A_t - \mu^*/\tan\beta|/m_{Q_3}$, and $\tan\beta$. Large values of these quantities tend to increase the Higgs mass at the expense of weakening the phase transition or the amount of baryon number produced. The allowed ranges have been found to be [18]

$$\begin{aligned} 5 &\lesssim \tan\beta \lesssim 10, \\ 0.3 &\lesssim |A_t - \mu^*/\tan\beta|/m_{Q_3} \lesssim 0.5. \end{aligned} \tag{6}$$

A strong electroweak phase transition is only a necessary condition for successful EWBG. In addition, a *CP* violating source is needed to generate a chiral charge asymmetry in the bubble walls. Within the MSSM, the dominant source is produced by the charginos, and is proportional to $\text{Im}(\mu M_2)$ [32,33]. For this source to be significant, the charginos must be abundant in the plasma, which requires that they not be too much heavier than the temperature of the plasma, $T \sim T_c$. In the recent analysis of Ref. [33], the authors found the bounds

$$\begin{aligned} |Arg(\mu M_2)| &\gtrsim 0.1, \\ \mu, M_2 &\lesssim 500 \text{ GeV}. \end{aligned} \tag{7}$$

These conditions are very relevant to the issue of neutralino dark matter.

The need for a large *CP* violating phase, Eq. (7), implies that there is a danger of violating the experimental bounds on the electric dipole moments (EDM) of the electron, neutron, and ^{199}Hg atom since phases generate new contributions to these EDM's. The leading contributions arise at one-loop order, and they all contain an intermediate first or second generation sfermion. They become negligible if these sfermions are very heavy, $m_{\tilde{f}} \gtrsim 10$ TeV. Such large masses have only a very small effect on EWBG. At two-loop order, if $Arg(\mu M_2) \neq 0$, there is a contribution involving an intermediate chargino and Higgs boson [34,35]. Since EWBG requires that this phase be nonzero and that the charginos be fairly light, the two-loop contribution is unavoidable if EWBG is to be successful. Thus, EDM limits strongly constrain the EWBG mechanism in the MSSM. Similarly, the branching ratio for $b \to s\gamma$ decays is also sensitive to this phase, and therefore imposes a further constraint on the EWBG mechanism.

[1]The requirements of a light stop and a light Higgs boson may be relaxed in nonminimal supersymmetric extensions. See, for instance, Refs. [23–30].

In a previous work [36], some of the present authors investigated the neutralino relic density in the presence of a light squark, as required for EWBG, but without including the effects of CP violating phases in the calculations. Here, we extend the analysis to study in detail the effect of phases in order to better understand the relationship between EWBG and dark matter within the MSSM. The outline of the paper is as follows. In Sec. II we investigate the relic density of a neutralino LSP in the presence of both a light stop and CP violating phases. Section III examines the prospects for direct detection of the neutralino dark matter in laboratory experiments, again including CP violating phases. In Sec. IV, we will look at the constraints on the phases needed for EWBG due to the electron EDM and flavour-violating $b \to s\gamma$ transitions. Finally, Sec. V is reserved for our conclusions.

II. NEUTRALINO DARK MATTER

As discussed in the introduction, the dual requirements of successful EWBG and a lightest Higgs boson with mass greater than the LEP II bounds strongly constrain the parameter space of the MSSM. One of the stops must be light, with mass less than that of the top, and mostly right handed. Furthermore, the charginos must not be too heavy, and the combination μM_2 must have a non-negligible phase. These conditions have important implications for neutralino dark matter.

First of all, if the lightest neutralino is to be the source of the observed dark matter, it must be lighter than the light stop so that it be stable. Secondly, in much of the parameter space of interest the light stop is only slightly heavier than the neutralino LSP implying that stop-neutralino coannihilation is significant. Finally, a phase for μM_2 modifies the masses of the neutralinos and their couplings to other particles, and can also affect the relative phase between the various contributions to the annihilation cross-section. The effect of CP violating phases on neutralino dark matter has been considered previously by several groups [37–40]. However, in all of these analyses the regions of MSSM parameter space considered were much different from the restricted subset required for EWBG, and, in particular, none of them included a light stop.

To simplify the analysis, we shall assume throughout this work that the gaugino mass parameters M_1 and M_2 are related by the standard unification relation, $M_2 = (g_2^2/g_1^2)M_1 \simeq 2M_1$. The stop soft parameters are largely fixed by the EWBG and Higgs mass conditions. We take them to be

$$\begin{aligned} m_{U_3}^2 &\approx 0 \qquad m_{Q_3} = 1.5 \text{ TeV} \\ |\mathrm{X_t}| &= |\mathrm{A_t} - \mu^*/\tan\beta| = 0.7 \text{ TeV}. \end{aligned} \tag{8}$$

We also set $m_{D_3} = m_{L_3} = m_{E_3} = 1$ TeV. EWBG and the Higgs mass constraint also require $5 \lesssim \tan\beta \lesssim 10$ and $M_A \gtrsim 200$ GeV. For concreteness, we shall consider the values

$$\begin{aligned} \tan\beta &= 7 \\ M_A &= 200, 1000 \text{ GeV}. \end{aligned} \tag{9}$$

The first and second generation sfermion soft masses are taken to be very large, $m_{\tilde{f}} \gtrsim 10$ TeV. As we will discuss in Sec. IV, this is necessary to avoid the electron, neutron, and ^{199}Hg EDM constraints in the presence of large phases.

The only phase that we consider in this work is the one directly related to EWBG, namely $Arg(\mu M_2)$. We will assume further that this phase is the result of a common phase for the gaugino mass parameters. With this assumption, all CP violating effects are confined to the chargino and neutralino sectors, or the loop corrections induced by them.[2] By means of a $\mathrm{U}(1)_R$ transformation, we may transfer the gaugino phase into the μ parameter and the trilinear A_f terms. Under this transformation, the effective values of these parameters are shifted according to

$$\begin{aligned} M_\lambda &\to M_\lambda e^{-i\varphi}, \\ \mu &\to \mu e^{i\varphi}, \\ A_f &\to A_f e^{-i\varphi}, \end{aligned} \tag{10}$$

with the remaining MSSM parameters left unchanged. For consistency of notation with [33], we will implicitly make a $\mathrm{U}(1)_R$ rotation such that the gaugino masses are all real and positive, and the μ parameter and the A_f terms have equal and opposite phases (up to a possible relative sign).

As a further simplification, we will neglect the mixing between CP-even and CP-odd Higgs bosons due to these phases. While this mixing can be significant in some regions of the MSSM parameter space, especially for large values of $\tan\beta$, $|\mu|$ and $|A_t|$, and small M_{H^+} [41], we have checked that the mixing (induced by chargino and neutralino loop corrections) is small ($\lesssim 3\%$) for the parameters considered here, where $\tan\beta$ takes only moderate values and the only relevant phase is the one associated with the gaugino sector. We also note that in [39] the effect of Higgs mixing on the neutralino relic density was found to be small, even in the large $\tan\beta$ regime, where the Higgs boson mixing is much larger. The supersymmetric corrections to the bottom mass [42] are also suppressed in the region of parameter space considered here, and hence all relevant CP violating effects are associated with the tree-level effect on the neutralino masses and couplings.

A. Relic density

We compute the relic abundance of neutralinos by numerically solving the Boltzmann equation,

[2] We do not consider the effects of a gluino phase. For the parameters considered in the present work, we expect that such a phase would only have a very small effect.

$$\frac{dn}{dt} = -3Hn - \langle \sigma_{eff} v \rangle (n^2 - n_{eq}^2), \tag{11}$$

for the number density of the supersymmetric particles $n = \sum_{i=1}^{N} n_i$. Because of conservation of R parity, the present value of n is equal to the number density of the lightest neutralino n_1. In Eq. (11) $H = 100h$ km/sec/Mpc, n_{eq} is the value of n at thermal equilibrium, and

$$\langle \sigma_{eff} v \rangle (x) = \frac{\int_2^\infty K_1(ax) \sum_{i,j=1}^{N} \lambda(a^2, b_i^2, b_j^2) g_i g_j \sigma_{ij}(a) da}{\frac{4}{x} (\sum_{i=1}^{N} K_2(b_i x) b_i^2 g_i)^2} \tag{12}$$

is the thermally averaged annihilation cross section. This quantity is a function of $x = m_1/T$, and is given in terms of the individual annihilation cross sections $\sigma_{ij}(a)$ of the processes $ij \to$ SM and/or Higgs particles. The energy and mass fractions $a = \sqrt{s}/m_1$ and $b_i = m_i/m_1$ also enter via $\lambda(a^2, b_i^2, b_j^2) = a^4 + b_i^4 + b_j^4 - 2(a^2 b_i^2 + a^2 b_j^2 + b_i^2 b_j^2)$. In Eq. (12) g_i is the number of degrees of freedom of the ith supersymmetric partner, and K_l is the modified Bessel function of the second kind of order l. The mass of the lightest neutralino is denoted by m_1.

In our calculation all relevant annihilation and coannihilation processes are included as described in Ref. [43]. Besides neutralino self-annihilations, coannihilations of the lightest neutralino with the lightest stop and the lighter chargino, and annihilations of the lightest stop and chargino effect significantly our numerical results. The complex phases enter our relic density calculation directly through the couplings and indirectly through the masses of the neutralinos and charginos. After diagonalization of the gaugino and sfermion complex mass matrices, we calculate the annihilation cross sections with complex couplings. In doing this, we follow techniques used in Refs. [44,45].

Figs. 1–3 show the dependence of the neutralino relic density on $|\mu|$ and M_1 for $\tan\beta = 7$, $M_A = 200$ GeV (left) and $M_A = 1000$ GeV (right), and three values of the μ phase: $Arg(\mu) = 0, \pi/2, \pi$. Values of the phase equal to 0 or π are representative of what happens for small phases, like the ones consistent with the generation of the baryon asymmetry when $|\mu| \simeq M_2$ and $M_A \lesssim 300$ GeV where there is a resonance in the amount of baryon number produced [33]. On the other hand, large values of the phase, close to $\pi/2$, tend to be necessary to generate the baryon asymmetry outside of the resonant region, particularly for large values of M_A, for which the EDM constraints become less severe.

The green (medium gray) bands in Figs. 1–3 show the region of parameter space where the neutralino relic density is consistent with the 95% CL limits set by WMAP data. The regions in which the relic density is above the experimental bound and excluded by more than 2 standard deviations are indicated by the red (dark gray) areas. The yellow (light gray) areas show the regions of parameter

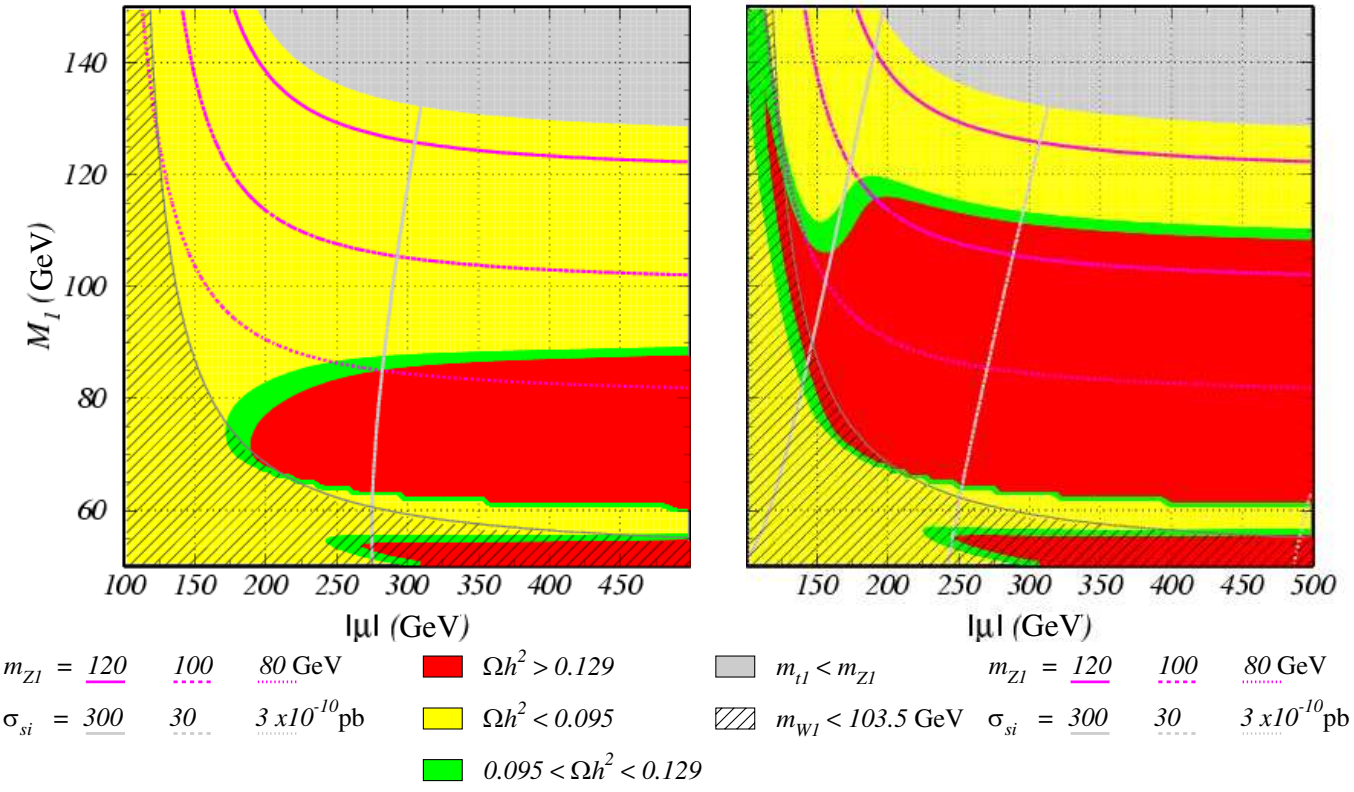

FIG. 1 (color online). Neutralino relic density for $M_A = 200$ GeV (left) and $M_A = 1000$ GeV (right), and $Arg(\mu) = 0$.

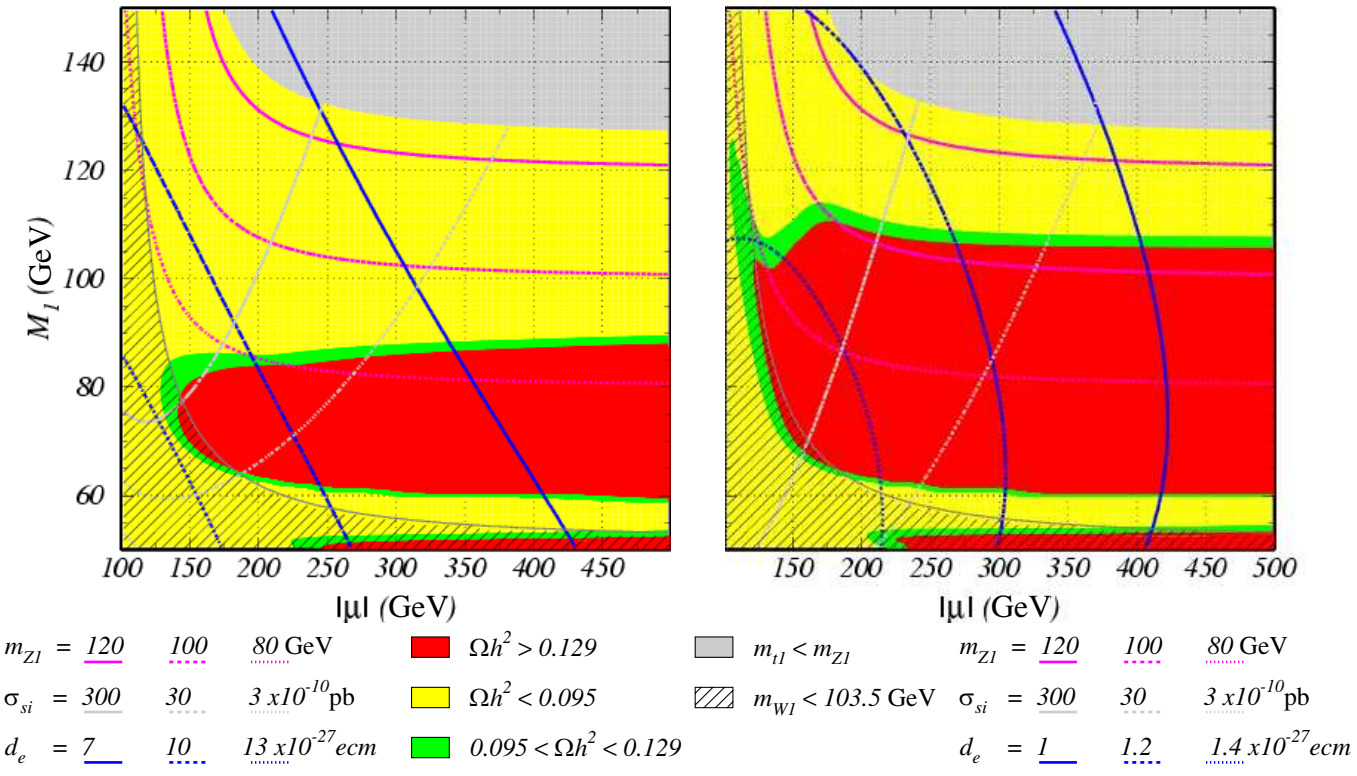

FIG. 2 (color online). Neutralino relic density for $M_A = 200$ GeV (left) and $M_A = 1000$ GeV (right), and $Arg(\mu) = \pi/2$.

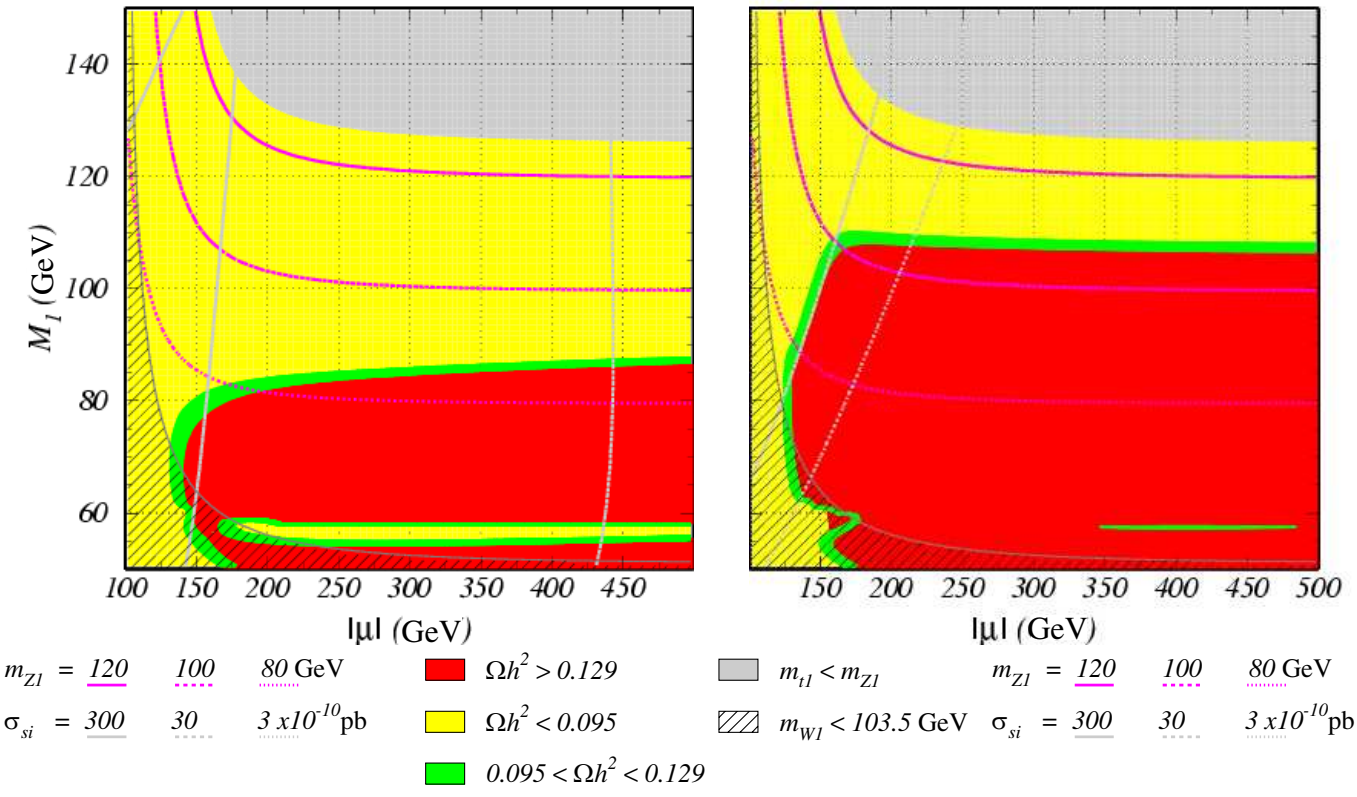

FIG. 3 (color online). Neutralino relic density for $M_A = 200$ GeV (left) and $M_A = 1000$ GeV (right), and $Arg(\mu) = \pi$.

space in which the neutralino relic density is less than the WMAP value. An additional source of dark matter, unrelated to the neutralino relic density, would be needed in these regions. Finally, in the (medium-light) gray region at the upper right the lightest stop becomes the LSP, while in the hatched area at the lower left corner the mass of the lightest chargino is lower than is allowed by LEP data [46].

These figures are qualitatively similar, but do show some differences due to the change in the phase of μ. Before discussing the effect of the phase, we will examine the general features of Figs. 1–3. For $M_A = 1000$ GeV and for all three phase values, the region where the relic density is too high consists of a wide band in which the lightest neutralino has mass between about 60 and 105 GeV and is predominantly Bino. Above this band, the mass difference between the neutralino LSP and the light stop is less than about 20 GeV, and stop-neutralino coannihilation as well as stop-stop annihilation are very efficient at reducing the neutralino abundance. For $M_A = 200$ GeV, instead, the contribution to neutralino annihilation from s-channel exchange of heavy CP-even and CP-odd Higgs bosons is enhanced by a resonance around $m_{\tilde{Z}_1} \simeq 100$ GeV. This restricts the band in which the relic density is too high to the region where the lightest neutralino has mass between about 60 and 85 GeV, and is also mostly Bino. For both values of M_A, there is an area below the disallowed band in which the neutralino mass lies in the range 40–60 GeV, and the neutralino annihilation cross-section is enhanced by resonances from s-channel h^0 and Z^0 exchanges.

The relic density is also quite low for smaller values of $|\mu|$. In these regions, the neutralino LSP acquires a significant Higgsino component allowing it to couple more strongly to the Higgs bosons and the Z^0. For $M_A = 1000$ GeV, this is particularly important in the region near $(|\mu|, M_1) = (175, 110)$ GeV where the neutralino mass becomes large enough that annihilation into pairs of gauge bosons through s-channel Higgs and Z^0 exchange and t-channel neutralino and chargino exchange is allowed, and is the reason for the dip in the relic density near this point. Since the corresponding couplings to the gauge bosons depend on the Higgsino content of the neutralino, these decay channels turn off as $|\mu|$ increases. For higher M_1 values, the lightest neutralino and chargino masses are also close enough that chargino-neutralino coannihilation and chargino-chargino annihilation substantially increase the effective cross section.

In Figures (1–3), we have taken $M_2 = (g_2^2/g_1^2)M_1$, as suggested by universality. Because of this, smaller values of M_1 and μ are excluded by the lower bound on the chargino mass from LEP data [46], as indicated by the hatched regions in the figures. This constraint becomes much less severe for larger values of the ratio M_2/M_1. We also find that increasing this ratio of gaugino masses (with M_1 held fixed) has only a very small effect on the neutralino relic density.

B. Effects of CP violating phases

For the parameters considered in the previous section, relevant for EWBG within the MSSM, CP violating phases modify the values of the neutralino relic density but have only a mild effect on the general qualitative features of the allowed parameter space. This is somewhat misleading, however, since the value of the relic density at a given point in the $|\mu| - M_1$ plane can vary markedly with $Arg(\mu)$.

The most important effect of varying $Arg(\mu)$ is to shift the mass of the neutralino LSP. The dependence of the lightest neutralino mass on this phase is shown in Fig. 4 for $\tan\beta = 7$ and three sample values of $(|\mu|, M_1)$: $(|\mu|, M_1) = (350, 110)$ GeV, $(300, 60)$ GeV, and $(175, 110)$ GeV. For $M_A = 1000$ GeV, these three points are representative of the regions where the annihilation cross section is dominated by stop-neutralino coannihilation ($(350, 110)$ GeV), Higgs boson s-channel annihilation ($(300, 60)$ GeV), and annihilation into pairs of gauge bosons ($(175, 110)$ GeV). In all three cases, the neutralino mass increases with $Arg(\mu)$, by about 3%, 7%, and 11%, respectively. Such a mass shift can significantly modify the relic density at a single point where neutralino annihilation is enhanced by a resonance or coannihilation with another species. The effect on the net distribution of relic densities, on the other hand, is fairly small; shifting the phase tends to translate this distribution down and to the left in the $|\mu|$–M_1 plane.

The neutralino-Higgs couplings are also quite sensitive to $Arg(\mu)$. The couplings of the Higgs bosons to a pair of neutralinos are given in [47], and have the form

$$\begin{aligned} \tilde{Z}_1\tilde{Z}_1 h^0/H^0 &\sim -i(FP_L + F^* P_R) \\ \tilde{Z}_1\tilde{Z}_1 A^0 &\sim -i(GP_L - G^* P_R) \end{aligned} \tag{13}$$

where $P_{L,R} = (1 \mp \gamma_5)/2$ are the usual chiral projectors. Using these vertices, the spin-summed and squared matrix elements for $\tilde{Z}_1\tilde{Z}_1 \to \bar{f}f$ annihilation via s-channel Higgs exchange are proportional to

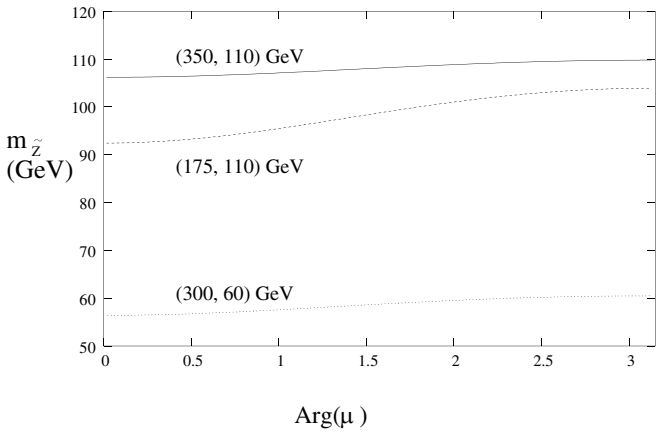

FIG. 4. Mass of the lightest neutralino as a function $Arg(\mu)$ for $\tan\beta = 7$ and three sample values of $(|\mu|, M_1)$.

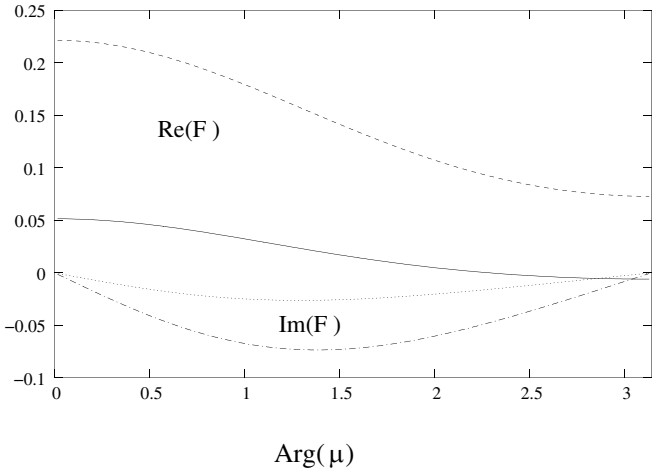

FIG. 5. Variation of the real and imaginary parts of the $\tilde{Z}_1\tilde{Z}_1h^0$ coupling with $Arg(\mu)$ for $(|\mu|, M_1) = (300, 60)$ GeV (solid and dotted), and $(|\mu|, M_1) = (175, 110)$ GeV (dashed and dash-dotted).

$$|\mathcal{M}|^2 \propto \begin{cases} \mathrm{Re}(F)^2(s - 4m_{\tilde{Z}_1}^2) + \mathrm{Im}(F)^2 s; & h^0, H^0 \\ \mathrm{Re}(G)^2 s + \mathrm{Im}(G)^2(s - 4m_{\tilde{Z}_1}^2); & A^0 \end{cases} . \quad (14)$$

In calculating the thermal average, one integrates these matrix elements over s through the range $[4m_{\tilde{N}}^2, \infty)$ with a Boltzmann factor, Eq. (12). The Boltzmann suppression is strong for a cold relic, so the integral is dominated by the region $s \sim 4m_{\tilde{N}}^2$. In particular, this means that the terms in Eq. (14) proportional to s have the potential to give a much larger contribution to the thermal average than those proportional to $(s - 4m_{\tilde{N}}^2)$.

The dependence of the $\tilde{Z}_1\tilde{Z}_1h^0$ coupling on $Arg(\mu)$ for $M_A = 1000$ GeV, and $(|\mu|, M_1) = (300, 60)$ GeV and $(|\mu|, M_1) = (175, 110)$ GeV is shown in Fig. 5. Both the real and imaginary parts of the couplings are larger in the $(|\mu|, M_1) = (175, 110)$ GeV case since for these values of the parameters, the neutralino LSP has a much larger Higgsino component than for $(|\mu|, M_1) = (300, 60)$ GeV, when the neutralino is mostly Bino. The couplings for $(|\mu|, M_1) = (350, 110)$ GeV, where the LSP is also mostly Bino, are very similar to those for $(|\mu|, M_1) = (300, 60)$ GeV. Setting $M_A = 200$ GeV has only a small effect on these couplings. For both points shown in Fig. 6, the imaginary part of the coupling vanishes when μ is real, and is largest when μ is pure imaginary, $Arg(\mu) = \pi/2$. The real part of the coupling also tends to decrease with $Arg(\mu)$ due to an accidental cancellation of terms. This behavior may be seen by comparing the region $M_1 \lesssim 60$ GeV in Figs. 1–3, where s-channel h^0 exchange tends to be dominant. The relic density in this region is lowest when $Arg(\mu) = \pi/2$, Fig. 2, while in Fig. 3, corresponding to $Arg(\mu) = \pi$, the contribution from h^0 exchange is much smaller than for other values of this phase.

The couplings of the H^0 and A^0 bosons to neutralinos are shown in Fig. 6 for $M_A = 1000$ GeV, and $(|\mu|, M_1) = (300, 60)$ GeV and $(|\mu|, M_1) = (175, 110)$ GeV. As with the h^0 coupling, these couplings are nearly unchanged when $M_A = 200$ GeV, and the couplings for $(|\mu|, M_1) = (350, 110)$ GeV are very similar to those for $(|\mu|, M_1) = (300, 60)$ GeV. The imaginary part of the H^0 and A^0 couplings vanishes for $Arg(\mu) = 0, \pi$ and is largest near $Arg(\mu) = \pi/2$, while the real parts of these couplings are largest for $Arg(\mu) = 0, \pi$ and nearly zero when $Arg(\mu) = \pi/2$. From Eqs. (13) and (14), this implies that the contribution of s-channel H^0 exchange to neutralino annihilation is largest when $Arg(\mu) = \pi/2$, and smallest for $Arg(\mu) = 0, \pi$, and that the opposite is true for s-channel A^0 exchange. Interestingly, the sum of the A^0 and H^0 contributions is nearly independent of the phase. We expect this to be the case whenever $M_A^2 \gg M_Z^2$, and the heavy CP-even and CP-odd Higgs states are nearly degenerate. The same effect was found in [39].

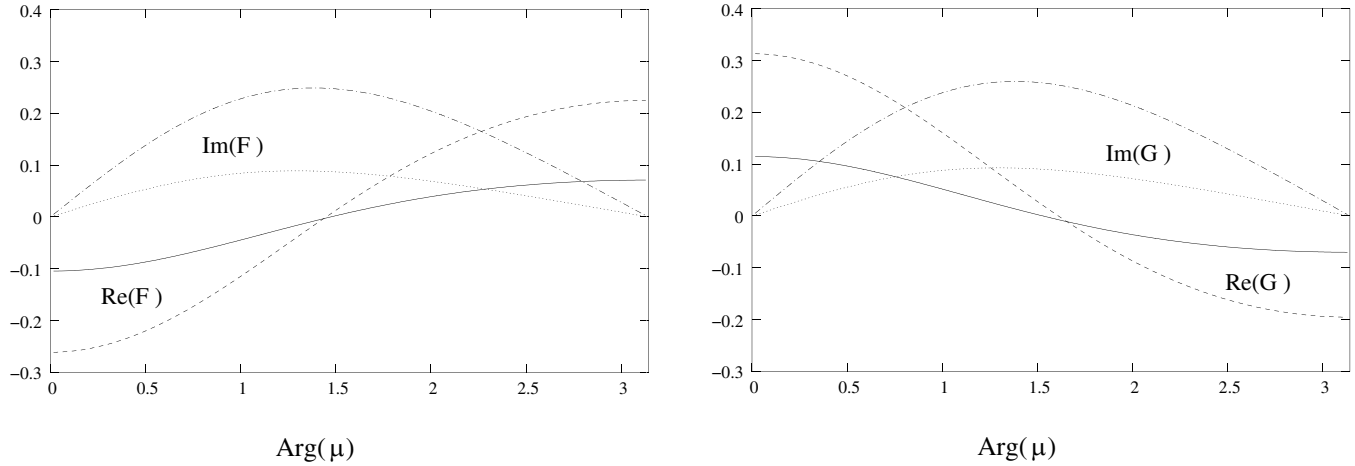

FIG. 6. Variation of the real and imaginary parts of the $\tilde{Z}_1\tilde{Z}_1H^0$ (left) and $\tilde{Z}_1\tilde{Z}_1A^0$ (right) couplings with $Arg(\mu)$ for $(|\mu|, M_1) = (300, 60)$ GeV (solid and dotted), and $(|\mu|, M_1) = (175, 110)$ GeV (dashed and dash-dotted).

We have also investigated the phase dependence of the $\tilde{Z}_1 t\tilde{t}$ coupling which generates the most important contributions to stop-neutralino coannihilation. While this coupling does vary somewhat with the phase, the effect of the phase on the neutralino mass is much more important. This is because the coannihilation contribution to the relic density is suppressed by a factor $e^{-(m_{\tilde{t}}-m_{\tilde{Z}_1})/T_f}$, where $T_f \simeq m_{\tilde{Z}_1}/20$ is the neutralino freeze-out temperature, making it very sensitive to the neutralino mass.

III. DIRECT DETECTION OF DARK MATTER

If space around us is filled with relic neutralinos, then it is plausible to try to observe them. Indeed, the search for weakly interacting massive particles is in progress via detection of their scattering off nuclei by measuring the nuclear recoil. Since neutralinos are nonrelativistic they can be directly detected via the recoiling off a nucleus in elastic scattering. There are several existing and future experiments engaged in this search. These include solid state germanium, ionization based detectors such as IGEX [48], HDMS [49], CDMS [50], EDELWEISS [51] and GENIUS [52]. Solid crystal or liquid NaI based scintillator detectors are used, for example, by DAMA [53] and ZEPLIN [54–57]. Liquid, gas or hybrid xenon based detector is used by experiments as XENON [58] and UKDMC [59]. Gas target projection chambers are utilized in DRIFT [60], and metastable particle detectors in SIMPLE [61] and PICASSO [62].

The elastic scattering interactions of neutralinos with nuclei can be described by the sum of spin-independent ($\mathcal{L}^{eff}_{\rm SI}$) and spin dependent ($\mathcal{L}^{eff}_{\rm SD}$) Lagrangian terms:

$$\mathcal{L}^{eff}_{\rm elastic} = \mathcal{L}^{eff}_{\rm SI} + \mathcal{L}^{eff}_{\rm SD}. \tag{15}$$

For heavy nuclei the spin-independent (SI) cross section, being proportional to the squared mass of the target nucleus, is highly enhanced compared to the spin dependent one. For the case of a target containing the isotope ^{127}I, for example, the enhancement factor is more than 10^4. For this reason the experimental limits on the spin-independent neutralino-nucleon cross sections are considerably stronger.

In what follows, we will focus on the spin-independent interactions of neutralinos with nuclei. At the parton level, these are mediated by t-channel Higgs and s-channel squark exchanges. (Here, we only consider the, so called, scalar contribution and neglect the higher order tensor contribution originating from loop diagrams.) The differential scattering rate of a neutralino off a nucleus X^A_Z with mass m_X takes the form [63]:

$$\frac{d\sigma_{\rm SI}}{d|\vec{q}|^2} = \frac{1}{\pi v^2}[Zf_p + (A-Z)f_n]^2 F^2(Q_r), \tag{16}$$

where $\vec{q} = \frac{m_X m_{\tilde{Z}_1}}{m_X + m_{\tilde{Z}_1}}\vec{v}$ is the three-momentum transfer, $Q_r = \frac{|\vec{q}|^2}{2m_N}$, and $F^2(Q_r)$ is the scalar nuclear form factor, $\vec{v}$ is the velocity of the incident neutralino and f_p and f_n are effective neutralino couplings to protons and neutrons, respectively. The same formalism was used in Ref. [63] to calculate neutralino-nucleon cross sections, and the reader is directed there for further details. Since modern experiments express their limits in terms of the neutralino-proton cross section, we calculate and plot this quantity in this work.

To study the dependence of the neutralino-proton cross section on complex phases of various supersymmetric parameters, we select a point in the examined parameter region where constraints from EWBG, the electron EDM and WMAP are simultaneously satisfied. Specifically, we examine values of $M_A = 200, 1000$ GeV and the same Higgsino and neutralino mass parameters chosen before, namely $(|\mu|, M_1) = (175, 110)$ GeV, (350,110) GeV and (300,60) GeV. As emphasized before, for $M_A = 1000$ GeV these points correspond to regions in which the annihilation cross section is dominated by weak processes, coannihilation with the light stop, and s-channel Higgs exchange, respectively.

Figs. 7–9 show the neutralino-proton cross section versus the phase of μ for the selected parameter space points. The most striking feature of these plots is that the cross section is suppressed for nonvanishing phases and, except for $(|\mu|, M_1) = (175, 110)$ GeV with $M_A = 1000$ GeV, nearly vanishes for a given value of $Arg(\mu)$. This behavior follows from the phase dependence of the Higgs-neutralino couplings. In our case, t-channel h^0 and H^0 exchange diagrams generate the most important contributions to the spin-independent neutralino-nucleon elastic scattering cross section. (We checked that the only relatively light squark, the lightest stop, contributes only at the percent level via its s-channel diagram.) Furthermore, these contributions depend only on the real (scalar) part of the Higgs-neutralino couplings [64,65]; Re(F) in the notation

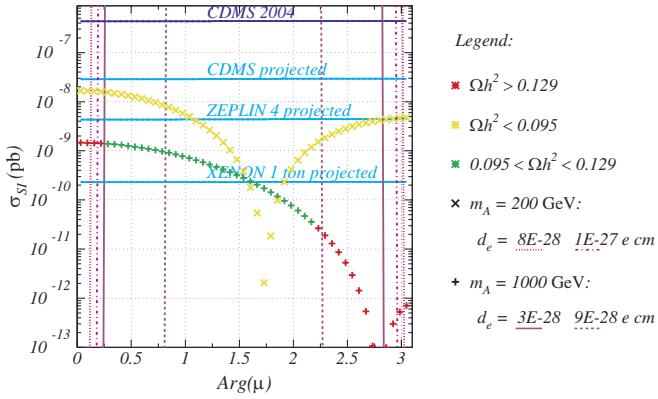

FIG. 7 (color online). Spin-independent neutralino-proton scattering cross section as the function of $Arg(\mu)$, for $|\mu| = 350$ GeV and $M_1 = 110$ GeV, and for $m_A = 200(1000)$ GeV for the upper (lower) curve.

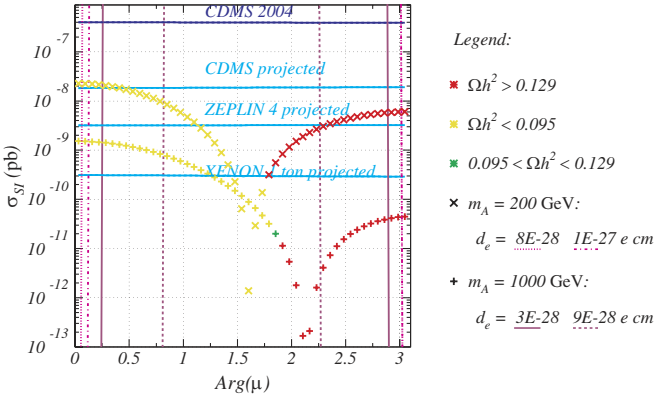

FIG. 8 (color online). Same as Fig. 7, but for $|\mu| = 300$ GeV and $M_1 = 60$ GeV.

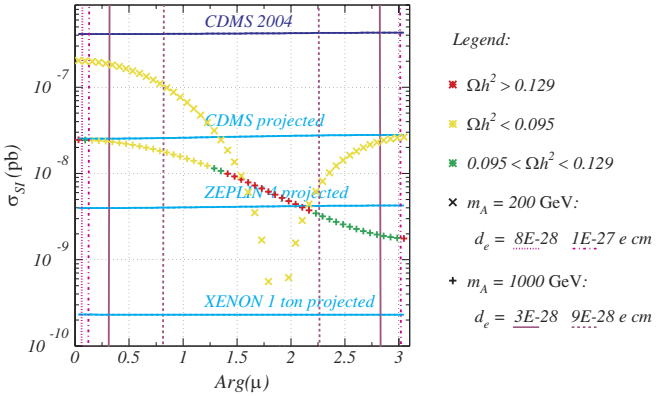

FIG. 9 (color online). Same as Fig. 7, but for $|\mu| = 175$ GeV and $M_1 = 110$ GeV.

of Eq. (13). The large suppression of the cross section for particular values of $Arg(\mu)$ is due to zeroes of $\mathrm{Re}(F)$.

Consider first the $M_A = 1000$ GeV lines in Figs. 7–9. For these, $M_A \simeq M_H \gg m_h$, so the contribution of the heavier scalar Higgs is suppressed relative to the lighter state, and the neutralino-proton scattering is dominated by t-channel h^0 exchange. Comparing the real part of the h^0-neutralino coupling for $(|\mu|, M_1) = (300, 60)$ GeV shown in Fig. 5 to the plot of σ_{SI} in Fig. 8 for $M_A = 1000$ GeV, we see that the minimum in σ_{SI} nearly coincides with the zero of the coupling. The minimum (not a zero value) in Fig. 8 does not exactly coincide with the zero of the coupling, but is shifted closer to $Arg(\mu) = \pi/2$ because the zero value of the real part of the H^0-neutralino coupling occurs close to $Arg(\mu) = \pi/2$, as shown in Fig. 6.[3] When $(|\mu|, M_1) = (175, 110)$ GeV, the coupling of the lightest Higgs to the lightest neutralino has no zero, and σ_{SI} has no deep minimum, as shown by Fig. 5. For $M_A = 200$ GeV, the H^0 state is much lighter and produces a much larger contribution to σ_{SI}. In this case, the minima of σ_{SI} are closer to $\pi/2$, near the zeroes of the H^0-neutralino coupling, as can be seen in Fig. 6.

The values of the electron EDM, to be discussed in the next section, are also indicated in Figs. 7–9. Among the direct detection experiments, CDMS excludes the region above the line labeled as CDMS 2004. The lower lines indicate the projected sensitivities of future experiments: CDMS [66], ZEPLIN [67] and XENON [68].

In Fig. 10, we examine the dependence of the direct dark-matter detection on the phase of μ. In order to do this, we conducted a random scan over the following range of MSSM parameters:

$$\begin{aligned} -(80\ \mathrm{GeV})^2 < m^2_{\tilde{U}_3} < 0, \\ 100\ \mathrm{GeV} < |\mu| < 500\ \mathrm{GeV}, \\ 50\ \mathrm{GeV} < M_1 < 150\ \mathrm{GeV}, \\ 200\ \mathrm{GeV} < M_A < 1000\ \mathrm{GeV}, \\ 5 < \tan\beta < 10. \end{aligned} \tag{17}$$

The parameters which are not scanned over are fixed as in Sec. II. The result of the scan, projected on the stop mass versus neutralino mass plane, is shown by Fig. 10. Here we plot $f\sigma_{\mathrm{SI}}$ as the function of the lightest neutralino mass, where

$$f = \begin{cases} \Omega_{\mathrm{CDM}}h^2/0.095 & \text{if} \quad 0.095 \geq \Omega_{\mathrm{CDM}}h^2 \\ 1 & \text{if} \quad 0.095 < \Omega_{\mathrm{CDM}}h^2 \end{cases} \tag{18}$$

accounts for the diminishing flux of neutralinos with their decreasing density [69].[4] For models marked by yellow (light gray) dots the neutralino relic density is below the 2 σ WMAP bound, while models represented by green (medium gray) dots comply with WMAP within 2 σ. Models that are above the WMAP value by more than 2 σ are indicated by red (dark gray) dots. The area indicated by hatching is excluded by the LEP chargino mass limit of 103.5 GeV. The top solid (blue) line represents the 2004 exclusion limit by CDMS [70]. The lower solid (cyan) lines indicate the projected sensitivity of the CDMS [66], ZEPLIN [67] and XENON [58] experiments.

The structure of this scatter plot is clear by examining Figs. 1–3. As shown on these plots by the gray direct detection contours, the spin-independent cross section, σ_{SI}, decreases for increasing values of $|\mu|$. Therefore,

[3]If the heavy Higgs state is decoupled completely, we find that the minimum of the scattering cross section coincides exactly with the zero of the h^0-neutralino coupling.

[4]The experimental limits for dark-matter detection rely on the standard assumptions of a dark-matter flux incident on the earth, based on the observational evidence that points to a roughly spherical distribution of dark-matter distribution in the galaxy, and a local dark-matter velocity comparable to the speed of the sun within the galaxy.

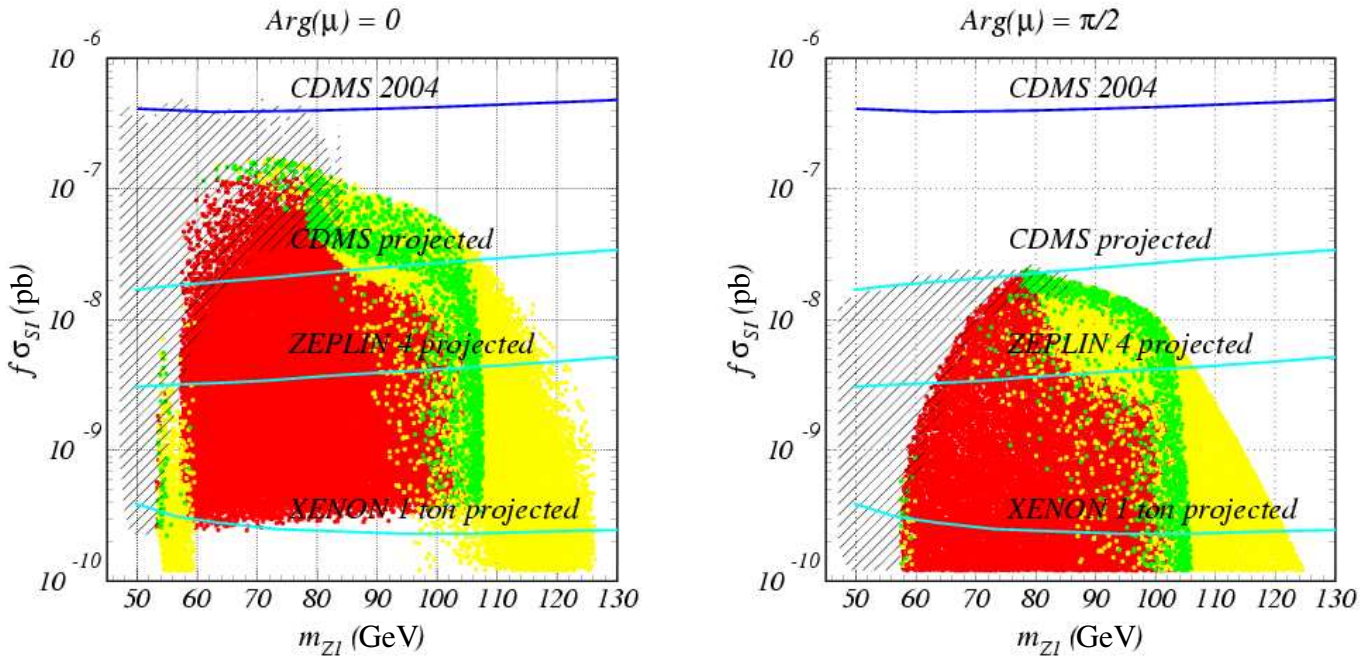

FIG. 10 (color online). Spin-independent neutralino-proton elastic scattering cross sections as a function of the neutralino mass for $Arg(\mu) = 0$ (left) and $Arg(\mu) = \pi/2$ (right). Red (dark gray), green (medium gray) and yellow (light gray) dots represent models in which the neutralino density is above, consistent or below the 2 σ WMAP bounds. Hatching indicates the region excluded by chargino searches at LEP. The top (blue) solid line represents the 2004 exclusion limit by CDMS. The lower solid (cyan) lines indicate the projected sensitivity of CDMS, ZEPLIN and XENON, respectively.

the low $\sigma_{\rm SI}$ region in Fig. 10 is in one to one correspondence with the large $|\mu|$ region in Figs. 1–3. For large values of $|\mu|$, the lightest neutralino mass is approximately given by M_1, hence, increasing values of M_1 in Figs. 1–3 correspond to increasing values of $m_{\tilde{Z}_1}$ in Fig. 10 and the same annihilation regions, via h^0 and A^0/H^0 resonances, and stop coannihilation regions of Figs. 1–3 can be identified in a clear way in Fig. 10. The LEP excluded, hatched area of $m_{\tilde{\chi}_1} < 103.5$ GeV, preserves its hyperbolic shape for $m_{\tilde{Z}_1} < 85$ GeV.

Presently, the region above the (blue) top solid line is excluded by CDMS. In the near future, for $Arg(\mu) = 0$, CDMS will probe part of the region of the parameter space where the WMAP dark-matter bound is satisfied. In this region, due to their enhanced Higgsino components, neutralinos mainly annihilate to gauge bosons or, due to the small mass gap, they coannihilate with charginos. The ZEPLIN experiment will start probing the stop-neutralino coannihilation region together with the annihilation region enhanced by s-channel A^0 resonances. Finally, XENON will cover most of the relevant parameter space. Prospects for direct detection of dark matter tend to be worse for large values of the phase of μ, $Arg(\mu) \simeq \pi/2$. As seen from Figs. 7–9, this phase can lead to cancellations which suppress the direct detection cross section. In the event of such a cancellation, a detector with the sensitivity of ZEPLIN is needed to start probing the parameter space, and not even XENON will be capable of fully exploring this model.

IV. CONSTRAINTS ON *CP* VIOLATING PHASES

A. Electron EDM constraints

The MSSM can accommodate many *CP* violating phases in addition to the CKM phase present in the SM. Such phases, however, are very highly constrained by the experimental limits on the electric dipole moments (EDM) of the electron, neutron, and ^{199}Hg atom. Of these, we will focus our attention on the electron EDM since it is the best measured, the least plagued by theoretical uncertainties, and for the phases relevant to the model under study gives the strongest constraint. The upper bound on the electron EDM comes from measurements of the EDM of the ^{205}Tl atom. For the phases considered in this work and in the absence of Higgs mixing, the *CP*-odd electron-neutron operator studied in [35] vanishes, and the ^{205}Tl EDM is due almost entirely to the electron EDM. This translates into a limit on the electron EDM of [71]

$$|d_e| < 1.6 \times 10^{-27} ecm, \tag{19}$$

at 90% CL.

In the MSSM, the leading order contributions to the electron EDM come from one-loop diagrams containing an intermediate selectron or sneutrino. For $\mathcal{O}(1)$ phases,

these loops generate an EDM well above the experimental limit unless these sfermions are taken to be quite heavy, $m_{\tilde{f}} \gtrsim 10$ TeV [72]. The neutron and ^{199}Hg EDM constraints require that the other first and second generation sfermions be very heavy as well. This feature arises in several models considered in the literature [30,73–75]. Such large first and second generation sfermion masses present no problem for EWBG since they couple very weakly to the Higgs bosons, and have only a minor effect on the final CP asymmetry [32]. With respect to EWBG, a much more dangerous contribution arises at two-loops.

At the two-loop order there are relevant contributions to the electron EDM from loops containing intermediate charginos and Higgs bosons. Since EWBG demands that the charginos be fairly light, $m_\chi \lesssim 500$ GeV, these contributions cannot be suppressed by taking large chargino masses. On the other hand, these terms can be reduced by taking large M_A or small $\tan\beta$. The phase associated with this contribution comes primarily from the chargino mass matrix, which is the same phase that generates the baryon asymmetry, and lower values of M_A can enhance the baryon asymmetry. Consequently, the electron EDM bound presents a particularly severe constraint on EWBG within the MSSM.

We have examined whether it is possible for EWBG to generate the observed baryon asymmetry while obeying the electron EDM bounds. The two-loop contributions to the electron EDM due to intermediate charginos and Higgs were calculated following [34,35]. The method of [33] was used to calculate the baryon asymmetry generated by EWBG. In our analysis, we have fixed $M_2 = 200$ GeV, and varied μ, $Arg(\mu)$, $\tan\beta$, and M_A. We also assume a bubble wall velocity of $v_w = 0.05$ and a wall width of $L_w = 20/T$. Both of these values are fairly typical, and tend to maximize the baryon asymmetry generated in the phase transition.

The dependence of the baryon asymmetry [relative to the value needed for big-bang nucleosynthesis (BBN)], $\eta/\eta_{\rm BBN}$, on $|\mu|$ and M_A is illustrated in Fig. 11. In this plot, we have taken the phase to be maximal, $\sin(Arg(\mu)) = 1$, and have set $\tan\beta = 5$. For other values of these parameters, the baryon asymmetry scales with $\sin(Arg(\mu))$ and (approximately) with $\sin 2\beta$. There are two main contributions from the CP violating currents of charginos and neutralinos to the baryon asymmetry in the MSSM. The first is proportional to the change in β going from the symmetric phase to the broken phase and exhibits a resonance at $M_2 = |\mu|$, but is highly suppressed for large values of M_A. The second contribution is independent of M_A, and falls off smoothly as $|\mu|$ becomes large. Both contributions go to zero as M_2 becomes large.

Figs. 12(a) and 12(b) show the regions in the $|\mu| - M_A$ and $M_A - \tan\beta$ planes consistent with both EWBG and the experimental bound on the electron EDM. Here, we have scanned over the ranges

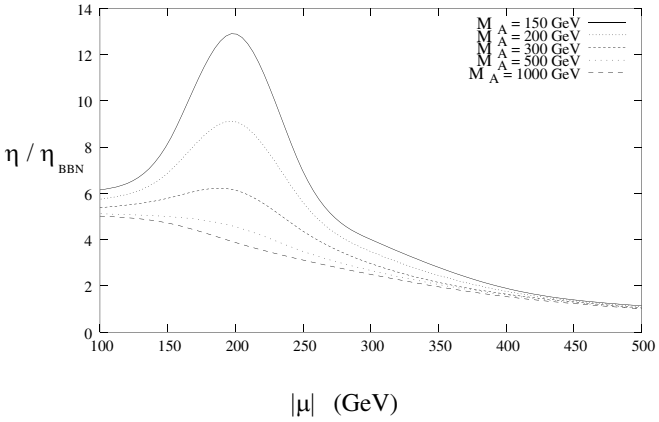

FIG. 11. Baryon asymmetry generated by EWBG relative to that required by big-bang nucleosynthesis for $M_2 = 200$, $\tan\beta = 5$, and $\sin(Arg(\mu)) = 1$.

$$\begin{aligned} 3 &< \tan\beta < 10, \\ 100\ \text{GeV} &< M_A < 1000\ \text{GeV}, \\ 100\ \text{GeV} &< |\mu| < 1000\ \text{GeV}, \end{aligned} \tag{20}$$

with $M_2 = 200$ GeV and the rest of the parameters as in Section II. In Fig. 12(a) we see that in the allowed region, $|\mu|$ is confined to the range $110 \lesssim |\mu| \lesssim 550$ GeV, while M_A must be greater than about 200 GeV. The limits on $|\mu|$ are due to the effect of this parameter on the chargino mass. For $|\mu| \lesssim 110$ GeV, the lighter chargino has mass below the experimental bound, $m_{\chi_1} \gtrsim 103.5$ GeV [46], while for large $|\mu|$, EWBG becomes less efficient. The lower bound on M_A arises for two reasons. For small M_A the two-loop contribution to the electron EDM is enhanced. At the same time the mass of the lightest Higgs is suppressed. The effect of the Higgs mass constraint can also be seen in Fig. 12(b), in which this bound results in a lower limit on $\tan\beta$. The allowed region is cut off for larger values of $\tan\beta$ since this tends to enhance the two-loop contributions to the electron EDM.

From Fig. 12, we see that it is possible to generate the baryon asymmetry via EWBG in the MSSM while satisfying the experimental constraints on the electron EDM and the mass of the lightest Higgs boson. Although this is reassuring, the EWBG scenario is still very strongly constrained by the electron EDM. This can be seen in Fig. 13, which shows the range of values of d_e obtained in our scan that are consistent with EWBG, the current electron EDM bound, and the Higgs mass limit. For $M_A < 1000$ GeV, an order of magnitude improvement of the electron EDM bound, $|d_e| < 0.2 \times 10^{-27} ecm$, will be sufficient to test this baryogenesis mechanism within the MSSM. However, we should also point out that the calculation of the baryon asymmetry from EWBG has $\mathcal{O}(1)$ uncertainties associated with the values of the bubble parameters, the wall velocity, and the derivative expansion used to derive the diffusion equations. Hence, the limits on EWBG presented here may

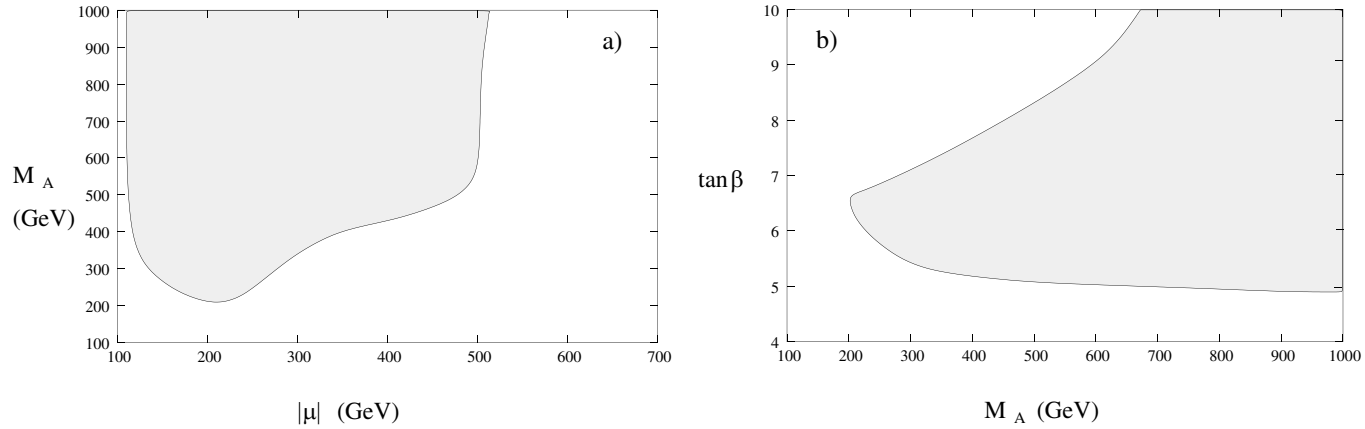

FIG. 12. Parameter regions consistent with EWBG and the electron EDM limit. In these plots, we have taken $M_2 = 200$ GeV and varied $Arg(\mu)$ over the interval $[0, \pi]$.

be somewhat more (or less) severe than they really are. Furthermore, we have not considered the possibility of fortuitous cancellations between different EDM contributions, for instance between the one-loop and two-loop terms (for lighter sfermions), which could further reduce the value of the electron EDM.

B. Constraints from BR(b→ sγ)

The presence of a light stop, light charginos, and a light charged Higgs boson may induce relevant effects on flavour changing neutral currents associated with the bottom quark [76]. One of the most sensitive experimental measurements of such effects is the branching ratio of the decay of a bottom quark into a strange quark and a photon [77–80]. A realistic calculation of these effects, however, cannot be performed without knowledge of the flavour sector of the theory. Even for the large values of the bottom squark masses we consider in this work, of order of a few TeV, the contributions coming from the interchange of gluinos and down squarks may be as large as the ones coming from the stop-chargino loops [81].

In the following, we shall present the results for the branching ratio of this rare decay, assuming that the only relevant contributions beyond the SM ones are those associated with the charged Higgs and stop-chargino loops. While the former tend to increase the BR($b \to s\gamma$) compared to the SM value, the latter has a nontrivial dependence on the CP violating phase. The experimental value of BR($b \to s\gamma$) is given by [82],

$$\mathrm{BR}(b \to s\gamma) = (3.54^{+0.30}_{-0.28}) \times 10^{-4}. \qquad (21)$$

In Fig. 14 we display the value of BR($b \to s\gamma$) as a function of the phase of the Higgsino mass parameter, μ, for $M_A = 200\,1000$ GeV. The stop sector parameters have been chosen as in Sec. II, while the chargino and neutralino mass parameters are taken to be $(|\mu|, M_1) = (300, 60)$ GeV (solid lines), (350,110) GeV (dashed lines), and (175,110) GeV (dotted lines).

As is apparent from the figure, in the absence of other sources of flavour violation, a light CP-odd Higgs scalar with mass of about 200 GeV is highly restricted by BR($b \to s\gamma$). Negative values of μX_t, where $X_t = A_t -$

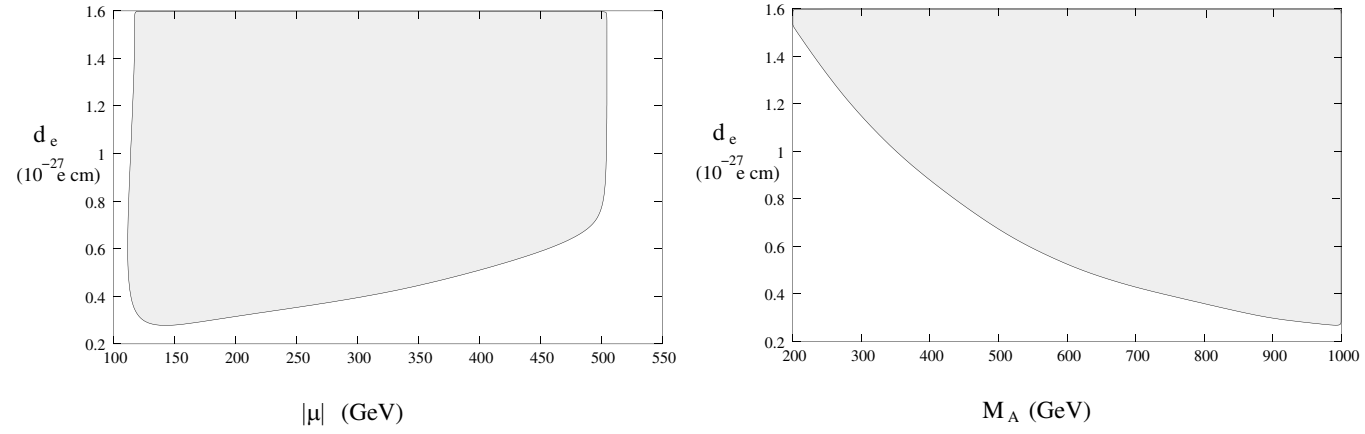

FIG. 13. Range of values of the electron EDM for parameter sets consistent with EWBG.

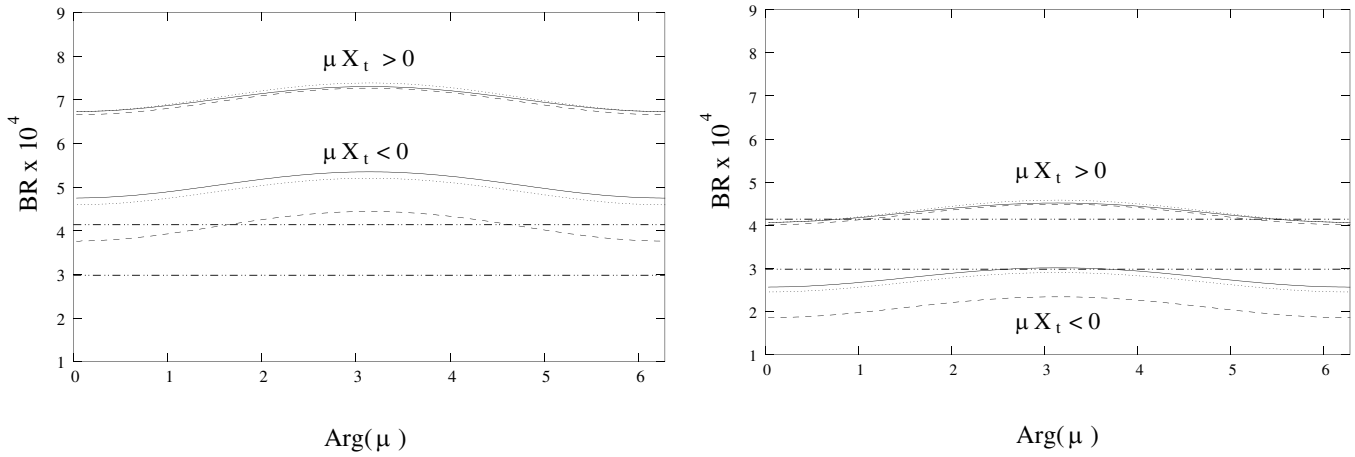

FIG. 14. BR($b \to s\gamma$) as a function of $Arg(\mu)$ for values of the CP-odd Higgs mass $M_A = 200$ GeV (left), and $M_A = 1000$ GeV (right). The stop parameters were chosen as in Sec. II, and the chargino and neutralino mass parameters are given by $(|\mu|, M_1) = (350, 110)$ GeV (solid lines), (175, 110) GeV (dashed lines), and (300, 60) GeV (dotted lines). The dot-dashed bands represent the present experimental range at the 2 σ level.

$\mu^*/\tan\beta$, are necessary to keep the predicted branching ratio close to the experimentally allowed range.[5] This is due to a cancellation between the charged Higgs and the squark-chargino contributions to the branching ratio when μX_t is negative. Otherwise these contributions interfere constructively with each other and with the SM contribution. For both signs of μX_t, the branching ratio is largest when $Arg(\mu) = \pi$ and smallest for $Arg(\mu) = 0$. Since the branching ratio tends to be somewhat high for $M_A \sim 200$ GeV, even with $\mu X_t < 0$, small values of $Arg(\mu)$ are preferred in this case.

Larger values of the CP-odd Higgs mass are consistent with the measured value of BR($b \to s\gamma$) over a wide range of values of M_1, μ, and $Arg(\mu)$. For moderately large values, $M_A \lesssim 1000$ GeV, negative $\mu X_t < 0$ is preferred. For $M_A \gtrsim 1000$ GeV, the charged Higgs contribution decouples leaving only the stop-chargino corrections. These corrections tend to give a branching ratio that is near the upper part ($\mu X_t > 0$) or lower part ($\mu X_t < 0$) of the experimentally allowed range for $|X_t| = 700$ GeV, as we have considered here. Thus, smaller $Arg(\mu)$ is preferred for $\mu X_t > 0$, while $Arg(\mu) \sim \pi$ is preferred for $\mu X_t < 0$. The chargino corrections can be reduced in size by taking slightly smaller values of $|X_t|$, or by invoking small flavour violation effects in the down squark sector.

V. CONCLUSIONS

Electroweak baryogenesis provides a mechanism for the generation of the baryon asymmetry that relies only on physics at the weak scale. It is therefore testable at high energy physics facilities in the near future. In a previous work, we showed that satisfactory dark-matter abundance may be obtained in the presence of a light stop like the one consistent with electroweak baryogenesis, and analyzed the impact of the allowed parameter space for stop searches at hadron colliders. No CP violating effects were considered.

In this work, we have analyzed the effect of CP violating phases, as required for EWBG, in conjunction with a light stop, with mass below the top-quark mass, and a light Higgs with mass below 120 GeV. We have shown that these phases have only a minor impact on the stop-neutralino parameter space leading to a consistent relic density. Large phases, however, have a relevant impact on direct dark-matter detection rates and induce large corrections to the electron electric dipole moment.

We have also shown that, for the phases necessary to obtain an acceptable baryon asymmetry and in the limit of heavy squarks, of order a few TeV, the predicted values of the electron electric dipole moment tend to lie within an order of magnitude below the reach of the present bounds. Even in the case of very heavy squarks, two-loop induced EDM's become relevant. Assuming no cancellations between one- and two-loop corrections, one can obtain strong bounds on the allowed parameter space: While small values of $\tan\beta$ are excluded since they lead to unacceptably small values of the Higgs mass, large values of $\tan\beta$ tend to lead to unacceptably large values of the electron EDM or small values of the baryon asymmetry. On the other hand, for moderate values of $\tan\beta \simeq 7$, the Higgs boson mass may be large enough to evade the LEP bounds, even for values of M_A as small as 200 GeV. For this particular value, and for $|\mu| \simeq M_2$, the baryon asymmetry may be large enough to be consistent with observations, even for small values of the phases, of order 0.1, for which the EDM's are consistent with the present experimental bounds.

[5]Recall that if the phases originate from a common gaugino phase and a $U(1)_R$ transformation is used to transfer this phase to μ and A_t, the product μA_t remains real but can have either sign. See Eq. (10).

In the above, we have not discussed the prospects of stop searches at hadron and lepton colliders. As discussed in Ref. [36], stop searches become very challenging in the region where stop-neutralino coannihilation becomes relevant, both at the LHC and the Tevatron collider [83], due to the small mass difference between the stop and the neutralino. An acceptable dark-matter density may be obtained for mass differences as small as 20 GeV, for which the charm particles proceeding from the stop decay are soft, making the stop detection difficult. As shown in Figs. 1–3, the presence of CP violating phases does not affect this result.

The linear collider signatures of MSSM Baryogenesis have been discussed in Ref. [76]. A linear collider represents the best possibility for confirming this scenario since it provides the opportunity of performing precise measurements of the chargino system and hence the possibility of observing a nonzero phase of the μ parameter [84]. Precise measurements of the stop system also become easier at a linear electron-positron collider [85]. For instance, the LEP collider was able to set limits on the stops even for a mass difference with the neutralino of about 1 GeV. Preliminary studies of stop searches at the linear collider [86] show that a 500 GeV ILC may be able to detect a light stop for mass differences as small as a few GeV. As said before, in the region of parameters where stop-neutralino coannihilation leads to a value of the relic density consistent with experimental results, the stop-neutralino mass difference is never much smaller than 20 GeV, and hence an ILC will be able to explore this region efficiently.

In summary, the requirement of a consistent generation of baryonic and dark matter in the MSSM leads to a well-defined scenario, where, apart from a light stop and a light Higgs boson, one has light neutralinos and charginos, sizeable CP violating phases, and moderate values of $5 \lesssim \tan\beta \lesssim 10$. All these properties will be tested by the Tevatron, the LHC and a prospective ILC, as well as through direct dark-matter detection experiments in the near future. The first tests of this scenario will come from electron EDM measurements, stop searches at the Tevatron and Higgs searches at the LHC within the next few years.

ACKNOWLEDGMENTS

M. C. and C. W. would like to thank M. Quiros and M. Seco for very useful discussions. We also gratefully acknowledge the use of JAZZ, a 350-node computing cluster operated by the Mathematics and Computer Science Division at ANL as part of its Laboratory Computing Resource Center. Work at ANL is supported in part by the US DOE, Division of HEP, Contract No. W-31-109-ENG-38. Fermilab is operated by Universities Research Association Inc. under Contract No. DE-AC02-76CH02000 with the DOE.

[1] WMAP Collaboration, D. N. Spergel *et al.*, Astrophys. J. Suppl. Ser. **148**, 175 (2003).
[2] SDSS Collaboration, M. Tegmark *et al.*, Phys. Rev. D **69**, 103501 (2004).
[3] H. E. Haber and G. L. Kane, Phys. Rep. **117**, 75 (1985); S. P. Martin, Phys. Rev. D **62**, 067505 (2000); H. P. Nilles, Phys. Rep. **110**, 1 (1984).
[4] A. D. Sakharov, Pis'ma Zh. Eksp. Teor. Fiz. **5**, 32 (1967) [JETP Lett. **5**, 24].
[5] J. M. Carmona, J. L. Cortes, A. Das, J. Gamboa, and F. Mendez, Phys. Usp. **44**, 871 (2001).
[6] For reviews, see: A. G. Cohen, D. B. Kaplan, and A. E. Nelson, Annu. Rev. Nucl. Part. Sci. **43**, 27 (1993); M. Quirós, Helv. Phys. Acta **67**, 451 (1994); V. A. Rubakov and M. E. Shaposhnikov, Phys. Usp. **39**, 461 (1996); M. Carena and C. E. M. Wagner, hep-ph/9704347; A. Riotto and M. Trodden, Annu. Rev. Nucl. Part. Sci. **49**, 35 (1999); M. Quirós and M. Seco, Nucl. Phys. B, Proc. Suppl. **81**, 63 (2000).
[7] G. 't Hooft, Phys. Rev. D **14**, 3432 (1976); **18**, 2199E (1978).
[8] N. S. Manton, Phys. Rev. D **28**, 2019 (1983); F. R. Klinkhamer and N. S. Manton, Phys. Rev. D **30**, 2212 (1984).
[9] D. Bodeker, Phys. Lett. B **426**, 351 (1998); P. Arnold and L. G. Yaffe, Phys. Rev. D **66**, 024019 (2002); P. Arnold, Phys. Rev. D **62**, 036003 (2000); G. D. Moore and K. Rummukainen, Phys. Rev. D **61**, 105008 (2000); G. D. Moore, Phys. Rev. D **62**, 085011 (2000).
[10] A. G. Cohen, D. B. Kaplan, and A. E. Nelson, Phys. Lett. B **336**, 41 (1994).
[11] P. Huet and A. E. Nelson, Phys. Rev. D **53**, 4578 (1996).
[12] A. I. Bochkarev and M. E. Shaposhnikov, Mod. Phys. Lett. A **2**, 417 (1987).
[13] K. Jansen, Nucl. Phys. B, Proc. Suppl. **47**, 196 (1996); K. Rummukainen, M. Tsypin, K. Kajantie, M. Laine, and M. Shaposhnikov, Nucl. Phys. **B532**, 283 (1998); K. Rummukainen, K. Kajantie, M. Laine, M. Shaposhnikov, and M. Tsypin, hep-ph/9809435.
[14] M. Carena, M. Quirós, and C. E. M. Wagner, Phys. Lett. B **380**, 81 (1996).
[15] M. Laine, Nucl. Phys. **B481**, 43 (1996); M. Losada, Phys. Rev. D **56**, 2893 (1997); G. Farrar and M. Losada, Phys. Lett. B **406**, 60 (1997).
[16] B. de Carlos and J. R. Espinosa, Nucl. Phys. **B503**, 24 (1997).
[17] D. Bodeker, P. John, M. Laine, and M. G. Schmidt, Nucl. Phys. **B497**, 387 (1997).

[18] M. Carena, M. Quiros, and C. E. M. Wagner, Nucl. Phys. **B524**, 3 (1998).
[19] M. Laine and K. Rummukainen, Nucl. Phys. **B535**, 423 (1998).
[20] M. Losada, Nucl. Phys. **B537**, 3 (1999); Nucl. Phys. **B569**, 125 (2000); M. Laine and M. Losada, Nucl. Phys. **B582**, 277 (2000).
[21] M. Laine and K. Rummukainen, Nucl. Phys. **B597**, 23 (2001).
[22] ALEPH Collaboration, R. Barate *et al.*, Phys. Lett. B **565**, 61 (2003).
[23] M. Pietroni, Nucl. Phys. **B402**, 27 (1993).
[24] A. T. Davies, C. D. Froggatt, and R. G. Moorhouse, Phys. Lett. B **372**, 88 (1996).
[25] S. J. Huber and M. G. Schmidt, Nucl. Phys. **B606**, 183 (2001).
[26] M. Bastero-Gil, C. Hugonie, S. F. King, D. P. Roy, and S. Vempati, Phys. Lett. B **489**, 359 (2000).
[27] J. Kang, P. Langacker, T. J. Li, and T. Liu, Phys. Lett. B **534**, 209 (2002).
[28] A. Menon, D. E. Morrissey and C. E. M. Wagner, Phys. Rev. D **70**, 035005 (2004).
[29] C. Grojean, G. Servant, and J. D. Wells, hep-ph/0407019.
[30] M. Carena, A. Megevand, M. Quiros, and C. E. M. Wagner, hep-ph/0410352.
[31] S. Heinemeyer, W. Hollik, and G. Weiglein, Phys. Rev. D **58**, 091701 (1998); S. Heinemeyer, W. Hollik, and G. Weiglein, Phys. Lett. B **440**, 296 (1998); S. Heinemeyer, W. Hollik, and G. Weiglein, Eur. Phys. J. C **9**, 343 (1999); M. Carena, M. Quiros, and C. E. M. Wagner, Nucl. Phys. B **461**, 407 (1996); H. E. Haber, R. Hempfling, and A. H. Hoang, Z. Phys. C **75**, 539 (1997); J. R. Espinosa and R. J. Zhang, J. High Energy Phys. 03 (2000) 026; J. R. Espinosa and R. J. Zhang, Nucl. Phys. **B586**, 3 (2000); M. Carena, H. E. Haber, S. Heinemeyer, W. Hollik, C. E. M. Wagner, and G. Weiglein, Nucl. Phys. **B580**, 29 (2000); G. Degrassi, P. Slavich, and F. Zwirner, Nucl. Phys. **B611**, 403 (2001); A. Brignole, G. Degrassi, P. Slavich, and F. Zwirner, hep-ph/0112177; S. P. Martin, Phys. Rev. D **67**, 095012 (2003).
[32] M. Carena, M. Quiros, A. Riotto, I. Vilja and C. E. M. Wagner, Nucl. Phys. **B503**, 387 (1997); J. M. Cline, M. Joyce, and K. Kainulainen, J. High Energy Phys. 07 (2000) 018; M. Carena, J. M. Moreno, M. Quiros, M. Seco, and C. E. Wagner, Nucl. Phys. **B599**, 158 (2001).
[33] M. Carena, M. Quiros, M. Seco, and C. E. M. Wagner, Nucl. Phys. **B650**, 24 (2003).
[34] D. Chang, W. F. Chang, and W. Y. Keung, Phys. Rev. D **66**, 116008 (2002).
[35] A. Pilaftsis, Nucl. Phys. **B644**, 263 (2002).
[36] C. Balazs, M. Carena, and C. E. M. Wagner, Phys. Rev. D **70**, 015007 (2004).
[37] T. Falk, K. A. Olive, and M. Srednicki, Phys. Lett. B **354**, 99 (1995).
[38] P. Gondolo and K. Freese, J. High Energy Phys. 07 (2002) 052.
[39] M. E. Gomez, T. Ibrahim, P. Nath, and S. Skadhauge, Phys. Rev. D **70**, 035014 (2004).
[40] M. Argyrou, A. B. Lahanas, D. V. Nanopoulos, and V. C. Spanos, Classical Quantum Gravity **18**, R1 (2001).
[41] A. Pilaftsis, Phys. Rev. D **58**, 096010 (1998); Phys. Lett. B **435**, 88 (1998); A. Pilaftsis and C. E. M. Wagner, Nucl. Phys. **B553**, 3 (1999); D. A. Demir, Phys. Rev. D **60**, 055006 (1999); S. Y. Choi, M. Drees, and J. S. Lee, Phys. Lett. B **481**, 57 (2000); M. Carena, J. Ellis, A. Pilaftsis, and C. E. M. Wagner, Nucl. Phys. **B586**, 92 (2000); G. L. Kane and L.-T. Wang, Phys. Lett. B **488**, 383 (2000); S. Y. Choi and J. S. Lee, Phys. Rev. D **61**, 015003 (2000); S. Y. Choi, K. Hagiwara, and J. S. Lee, Phys. Rev. D **64**, 032004 (2001); S. Y. Choi, M. Drees, J. S. Lee, and J. Song, Eur. Phys. J. C **25**, 307 (2002); T. Ibrahim and P. Nath, Phys. Rev. D **63**, 035009 (2001); Phys. Rev. D **66**, 015005 (2002); T. Ibrahim, Phys. Rev. D **64**, 035009 (2001); S. W. Ham, S. K. Oh, E. J. Yoo, C. M. Kim, and D. Son, hep-ph/0205244; M. Carena, J. Ellis, A. Pilaftsis, and C. E. M. Wagner, Phys. Lett. B **495**, 155 (2000); S. Heinemeyer, Eur. Phys. J. C **22**, 521 (2001); M. Carena, J. Ellis, S. Mrenna, A. Pilaftsis, and C. E. M. Wagner, Nucl. Phys. **B659**, 145 (2003); J. S. Lee, A. Pilaftsis, M. Carena, S. Y. Choi, M. Drees, J. R. Ellis, and C. E. M. Wagner, Comput. Phys. Commun. **156**, 283 (2004).
[42] R. Hempfling, Phys. Rev. D **49**, 6168 (1994); L. Hall, R. Rattazzi, and U. Sarid, Phys. Rev. D **50**, 7048 (1994); M. Carena, M. Olechowski, S. Pokorski, and C. E. M. Wagner, Nucl. Phys. **B426**, 269 (1994); D. Pierce, J. Bagger, K. Matchev, and R. Zhang, Nucl. Phys. **B491**, 3 (1997); M. Carena, D. Garcia, U. Nierste, and C. E. M. Wagner, Nucl. Phys. **B577**, 88 (2000).
[43] H. Baer, C. Balázs and A. Belyaev, J. High Energy Phys. 03 (2002) 042.
[44] P. Gondolo, J. Edsjo, P. Ullio, L. Bergstrom, M. Schelke, and E. A. Baltz, J. Cosmol. Astropart. Phys. 07 (2004) 008.
[45] S. Katsanevas and P. Morawitz, Comput. Phys. Commun. **112**, 227 (1998).
[46] LEP2 SUSY Working Group Combined LEP Chargino Results, up to 208 GeV, http://lepsusy.web.cern.ch/lepsusy/www/inos_moriond01/charginos_pub.html.
[47] J. F. Gunion, H. E. Haber, G. L. Kane, and S. Dawson, *The Higgs Hunter's Guide*, Report No. SCIPP-89/13.
[48] IGEX Collaboration, I. G. Irastorza *et al.*, Phys. Rev. D **69**, 124015 (2004).
[49] H. V. Klapdor-Kleingrothaus, A. Dietz, G. Heusser, I. V. Krivosheina, D. Mazza, H. Strecker, and C. Tomei, Astropart. Phys. **18**, 525 (2003).
[50] CDMS Collaboration, D. Abrams *et al.*, Phys. Rev. D **66**, 122003 (2002).
[51] A. Benoit *et al.*, Phys. Lett. B **545**, 43 (2002).
[52] H. V. Klapdor-Kleingrothaus, Nucl. Phys. B, Proc. Suppl. **110**, 364 (2002).
[53] R. Bernabei *et al.*, astro-ph/0205047.
[54] N. Spooner, in *Proceedings of the APS/DPF/DPB Summer Study on the Future of Particle Physics, Snowmass, 2001*, edited by N. Graf, eConf C010630, E601 (2001).
[55] D. Cline *et al.*, *Proceedings of the 3rd International Conference on Dark Matter in Astro and Particle Physics (Dark 2000), Heidelberg, Germany, 2000.*
[56] J. Dawson *et al.*, Nucl. Phys. B, Proc. Suppl. **110**, 109 (2002).
[57] D. B. Cline, H. G. Wang, and Y. Seo, in *Proceedings of the APS/DPF/DPB Summer Study on the Future of Particle Physics, Snowmass, 2001,* edited by N. Graf,

eConf C010630, E108 (2001); astro-ph/0108147.
[58] E. Aprile *et al.*, Nucl. Phys. B, Proc. Suppl. **138**, 156 (2005).
[59] UKDM Collaboration, and Boulby Collaboration, N. J. C. Spooner, *Proceedings of the International Workshop on Technique and Application of Xenon Detectors, Kashiwa, Japan, 2001*.
[60] N. Spooner, in *Proceedings of the APS/DPF/DPB Summer Study on the Future of Particle Physics, Snowmass, 2001*, edited by N. Graf, eConf C010630, P401 (2001).
[61] J. I. Collar, J. Puibasset, T. A. Girard, D. Limagne, H. S. Miley, and G. Waysand, New J. Phys. **2**, 14 (2000).
[62] N. Boukhira *et al.*, Nucl. Phys. B, Proc. Suppl. **110**, 103 (2002).
[63] H. Baer, C. Balázs, A. Belyaev, and J. O'Farrill, J. Cosmol. Astropart. Phys. 09 (2003) 007.
[64] S. Y. Choi, S. C. Park, J. H. Jang, and H. S. Song, Phys. Rev. D **64**, 015006 (2001).
[65] T. Nihei and M. Sasagawa, Phys. Rev. D **70**, 055011 (2004); **70**, 079901E (2004).
[66] CDMS Collaboration, L. Baudis, eConf C020805, TF02 (2002).
[67] D. B. Cline *et al.*, Nucl. Phys. B, Proc. Suppl. **124**, 229 (2003).
[68] E. Aprile, *Proceedings of the 6th UCLA Symposium on Sources and Detection of Dark Matter and Dark Energy in the Universe, Marina Beach Marriott, Marina del Rey, California, 2004*, http://www.physics.ucla.edu/hep/dm04/talks/aprile.pdf.
[69] J. R. Ellis, A. Ferstl, and K. A. Olive, Phys. Rev. D **63**, 065016 (2001).
[70] CDMS Collaboration, D. S. Akerib *et al.*, Phys. Rev. Lett. **93**, 211301 (2004);
[71] B. C. Regan, E. D. Commins, C. J. Schmidt, and D. DeMille, Phys. Rev. Lett. **88**, 071805 (2002).
[72] S. Abel, S. Khalil, and O. Lebedev, Nucl. Phys. B **606**, 151 (2001).
[73] A. G. Cohen, D. B. Kaplan, and A. E. Nelson, Phys. Lett. B **388**, 588 (1996).
[74] J. L. Feng, K. T. Matchev, and T. Moroi, Phys. Rev. D **61**, 075005 (2000).
[75] N. Arkani-Hamed, S. Dimopoulos, G. F. Giudice, and A. Romanino, Nucl. Phys. **B709**, 3 (2005).
[76] H. Murayama and A. Pierce, Phys. Rev. D **67**, 071702 (2003).
[77] S. Bertolini, F. Borzumati, A. Masiero, and G. Ridolfi, Nucl. Phys. **B353**, 591 (1991).
[78] R. Barbieri and G. F. Giudice, Phys. Lett. B **309**, 86 (1993); M. Ciuchini, G. Degrassi, P. Gambino and G. F. Giudice, Nucl. Phys. **B534**, 3 (1998).
[79] G. Degrassi, P. Gambino, and G. F. Giudice, J. High Energy Phys. 12 (2000) 009.
[80] M. Carena, D. Garcia, U. Nierste, and C. E. M. Wagner, Phys. Lett. B **499**, 141 (2001).
[81] F. Gabbiani, E. Gabrielli, A. Masiero, and L. Silvestrini, Nucl. Phys. **B477**, 321 (1996); K. I. M. Okumura and L. Roszkowski, J. High Energy Phys. 10 (2003) 024.
[82] ALEPH Collaboration, R. Barate *et al.*, Phys. Lett. B **429**, 169 (1998); CLEO Collaboration, S. Chen *et al.*, Phys. Rev. Lett. **87**, 251807 (2001); Belle Collaboration, K. Abe *et al.*, Phys. Lett. B **511**, 151 (2001); Belle Collaboration, P. Koppenburg *et al.*, Phys. Rev. Lett. **93**, 061803 (2004); BABAR Collaboration, B. Aubert *et al.*, hep-ex/0207074; hep-ex/0207076.
[83] R. Demina, J. D. Lykken, K. T. Matchev, and A. Nomerotski, Phys. Rev. D **62**, 035011 (2000);
[84] S. Y. Choi, J. S. Shim, H. S. Song, and W. Y. Song, hep-ph/9808227; S. Y. Choi, A. Djouadi, M. Guchait, J. Kalinowski, H. S. Song, and P. M. Zerwas, Eur. Phys. J. C **14**, 535 (2000); V. D. Barger, T. Falk, T. Han, J. Jiang, T. Li, and T. Plehn, Phys. Rev. D **64**, 056007 (2001).
[85] A. Bartl, S. Hesselbach, K. Hidaka, T. Kernreiter, and W. Porod, hep-ph/0306281.
[86] M. Carena, A. Finch, A. Freitas, C. Milstene, H. Novak, and A. Sopczak (unpublished).